

Long-wavelength-pumped upconversion single-photon detector at 1550 nm: performance and noise analysis

J. S. Pelc,^{1,*} L. Ma,² C. R. Phillips,¹ Q. Zhang,^{1,3} C. Langrock,¹
O. Slattery,² X. Tang,² and M. M. Fejer¹

¹*E. L. Ginzton Laboratory, Stanford University, Stanford, California, USA*

²*Information Technology Laboratory, National Institute of Standards and Technology,
Gaithersburg, Maryland, USA*

³*USTC Shanghai Institute for Advanced Studies, Shanghai, China*

*jpelc@stanford.edu

Abstract: We demonstrate upconversion-assisted single-photon detection for the 1.55- μm telecommunications band based on a periodically poled lithium niobate (PPLN) waveguide pumped by a monolithic PPLN optical parametric oscillator. We achieve an internal conversion efficiency of 86%, which results in an overall system detection efficiency of 37%, with excess noise as low as 10^3 counts s^{-1} . We measure the dark count rate versus the upconversion pump-signal frequency separation and find the results to be consistent with noise photon generation by spontaneous anti-Stokes Raman scattering. These results enable detailed design guidelines for the development of low-noise quantum frequency conversion systems, which will be an important component of fiber-optic quantum networks.

© 2011 Optical Society of America

OCIS codes: (040.5570) Quantum detectors; (190.7220) Upconversion; (270.5565) Quantum communications; (290.5860) Scattering, Raman.

References and links

1. N. Namekata, H. Takesue, T. Honjo, Y. Tokura, and S. Inoue, "High-rate quantum key distribution over 100 km using ultra-low-noise, 2-GHz sinusoidally gated InGaAs/InP avalanche photodiodes," *Opt. Express* **19**, 10632–10639 (2011).
2. R. H. Hadfield, "Single-photon detectors for optical quantum information applications," *Nat. Photonics* **3**, 696–705 (2009).
3. R. E. Warburton, M. Itzler, and G. S. Buller, "Free-running, room temperature operation of an InGaAs/InP single-photon avalanche diode," *Appl. Phys. Lett.* **94**, 071116 (2009).
4. G. N. Gol'tsman, O. Okunev, G. Chulkova, A. Lipatov, A. Semenov, K. Smirnov, B. Voronov, A. Dzardanov, C. Williams, and R. Sobolewski, "Picosecond superconducting single-photon optical detector," *Appl. Phys. Lett.* **79**, 705–707 (2001).
5. B. Cabrera, R. M. Clarke, P. Colling, A. J. Miller, S. Nam, and R. W. Romani, "Detection of single infrared, optical, and ultraviolet photons using superconducting transition edge sensors," *Appl. Phys. Lett.* **73**, 735–737 (1998).
6. A. P. Vandevender and P. G. Kwiat, "High efficiency single photon detection via frequency up-conversion," *J. Mod. Opt.* **51**, 1433–1445 (2004).
7. P. Kumar, "Quantum frequency conversion," *Opt. Lett.* **15**, 1476–1478 (1990).
8. C. Langrock, E. Diamanti, R. V. Roussev, Y. Yamamoto, M. M. Fejer, and H. Takesue, "Highly efficient single-photon detection at communication wavelengths by use of upconversion in reverse-proton-exchanged periodically poled LiNbO₃ waveguides," *Opt. Lett.* **30**, 1725–1727 (2005).
9. M. A. Albota and F. N. C. Wong, "Efficient single-photon counting at 1.55 μm by means of frequency upconversion," *Opt. Lett.* **29**, 1449–1451 (2004).

10. A. P. VanDevender and P. G. Kwiat, "Quantum transduction via frequency upconversion," *J. Opt. Soc. Am. B* **24**, 295–299 (2007).
11. S. Tanzilli, W. Tittel, M. Halder, O. Alibart, P. Baldi, N. Gisin, and H. Zbinden, "A photonic quantum information interface," *Nature* **437**, 116–120 (2005).
12. M. T. Rakher, L. Ma, O. Slattery, X. Tang, and K. Srinivasan, "Quantum transduction of telecommunications-band single photons from a quantum dot by frequency upconversion," *Nat. Photonics* **4**, 786–791 (2010).
13. H. Takesue, "Erasing distinguishability using quantum frequency up-conversion," *Phys. Rev. Lett.* **101**, 173901 (2008).
14. L. Ma, M. T. Rakher, M. J. Stevens, O. Slattery, K. Srinivasan, and X. Tang, "Temporal correlation of photons following frequency up-conversion," *Opt. Express* **19**, 10501–10510 (2011).
15. J. S. Pelc, C. R. Phillips, D. Chang, C. Langrock, and M. M. Fejer, "Efficiency pedestal in quasi-phase-matching devices with random duty-cycle errors," *Opt. Lett.* **36**, 864–866 (2011).
16. J. S. Pelc, C. Langrock, Q. Zhang, and M. M. Fejer, "Influence of domain disorder on parametric noise in quasi-phase-matched quantum frequency converters," *Opt. Lett.* **35**, 2804–2806 (2010).
17. M. Maljy and J. E. Griffiths, "Stokes/Anti-Stokes Raman vibrational temperatures: reference materials, standard lamps, and spectrophotometric calibrations," *Appl. Spectrosc.* **37**, 315–333 (1983).
18. S. Zaske, A. Lenhard, and C. Becher, "Efficient frequency downconversion at the single photon level from the red spectral range to the telecommunications C-band," *Opt. Express* **19**, 12825–12836 (2011).
19. H. Dong, H. Pan, L. Yao, E. Wu, and H. Zeng, "Efficient single-photon frequency upconversion at 1.06 μm with ultralow background counts," *Appl. Phys. Lett.* **93**, 071101 (2008).
20. H. Kamada, M. Asobe, T. Hongo, H. Takesue, Y. Tokura, Y. Nishida, O. Tadanaga, and H. Miyazawa, "Efficient and low-noise single-photon detection in 1550 nm communication band by frequency upconversion in periodically poled LiNbO₃ waveguides," *Opt. Lett.* **33**, 639–641 (2008).
21. H. J. Kimble, "The quantum internet," *Nature (London)* **453**, 1023–1030 (2008).
22. Z. Y. Ou, "Efficient conversion between photons and between photon and atom by stimulated emission," *Phys. Rev. A* **78**, 023819 (2008).
23. R. Regener and W. Sohler, "Loss in low-finesse Ti:LiNbO₃ optical waveguide resonators," *Appl. Phys. B* **36**, 143–147 (1985).
24. C. R. Phillips, J. S. Pelc, and M. M. Fejer, "Continuous wave monolithic quasi-phaseshifted optical parametric oscillator in periodically poled lithium niobate," *Opt. Lett.* **36**, 2973–2975 (2011).
25. H. Takesue, E. Diamanti, C. Langrock, M. M. Fejer, and T. Yamamoto, "1.5- μm single photon counting using polarization-independent up-conversion detector," *Opt. Express* **14**, 13067–13072 (2006).
26. A Single Photon Counting Module Datasheet, SPCM-QR Series (PerkinElmer, 2004), pp. 1-10.
27. D. H. Jundt, "Temperature-dependent Sellmeier equation for the index of refraction, n_e , in congruent lithium niobate," *Opt. Lett.* **22**, 1553–1555 (1997).
28. R. W. Boyd, *Nonlinear Optics*, 3rd ed. (Academic, 2008).
29. M. Meleshkevich, A. Drozhzhin, N. Platonov, D. Gapontsev, and D. Starodubov, "10 W single-mode single-frequency Tm-doped fiber amplifiers optimized for 1800-2020-nm band," *Proc. SPIE* **5709**, 117–124 (2005).
30. Shibin Jiang, private communication (2011).
31. R. Loudon, "The Raman effect in crystals," *Adv. Phys.* **50**, 813–864 (2001).
32. Y. R. Shen, *The Principles of Nonlinear Optics*, (Wiley-Interscience, 1984).
33. L. Ma, Jo. C. Bienfang, O. Slattery, and X. Tang, "Up-conversion single-photon detector using multi-wavelength sampling techniques," *Opt. Express* **19**, 5470–5479 (2011).

1. Introduction

Single-photon detectors (SPDs) play a critical role in quantum communication systems; for implementations of quantum key distribution (QKD) over fiber-optic networks, the maximum reach and data rate are limited by the performance of SPDs for the 1.5 μm low-loss window of silica fiber [1]. Current commercial detectors in this spectral window are most often based on InGaAs/InP avalanche photodiodes (APDs) [2]. Whereas Si APDs can have photon detection efficiencies (PDEs) exceeding 70% with dark count rates (DCRs) lower than 10 s^{-1} , InGaAs/InP APDs typically have PDEs closer to 20%. Furthermore, the latter are typically gated to avoid dark counts due to afterpulsing, and usually have DCRs greater than 10^4 s^{-1} . Although free-running InGaAs/InP SP detectors have recently been demonstrated [3], they have low PDE and high DCR prohibitive for use in QKD systems. There has also been recent progress on superconducting SPDs either as transition-edge sensors or superconducting nanowire detectors [4,5]. Although these two technologies have impressive performance, they are of potentially limited

field utility due to the need for bulky cryogenic cooling and exquisite temperature control.

Upconversion-assisted SPDs offer a technique by which one may extend the spectral range of Si-based SPDs into the telecommunications band near 1.55 μm [6]. They are based on the concept of quantum frequency conversion (QFC), in which it can be shown that frequency conversion in $\chi^{(2)}$ media by either sum- or difference-frequency generation (SFG/DFG) can interchange quantum states of light between two frequencies ω_1 and ω_2 via interaction with a strong optical pump at ω_p , with $\omega_1 + \omega_p = \omega_2$ [7]. The efficiency of the conversion process for a waveguide of length L with negligible propagation loss and a phase-matched interaction is given by

$$\eta = \frac{\langle N_2(z=L) \rangle}{\langle N_1(z=0) \rangle} = \sin^2(\sqrt{\eta_{\text{nor}} P_p L}) \quad (1)$$

where N_j is the photon number operator and P_p is the pump power [8]. The normalized efficiency η_{nor} is given by

$$\eta_{\text{nor}} = \varepsilon_0^2 d_{\text{eff}}^2 |\theta_Q|^2 \frac{2\omega_1 \omega_2 Z_0^3}{n_p n_1 n_2}, \quad (2)$$

where d_{eff} is the effective nonlinear coefficient, $Z_0 = \sqrt{\mu_0/\varepsilon_0}$ is the impedance of free space, n_j are the effective indices of refraction, and θ_Q is the mode-overlap integral for three-wave interactions:

$$\theta_Q = \iint_{-\infty}^{\infty} \bar{d}(x,y) u_1(x,y) u_p(x,y) u_2^*(x,y) dx dy. \quad (3)$$

Here, the $u_j(x,y)$ are modal field profiles with normalization $\iint |u_j(x,y)|^2 dx dy = 1$, and $\bar{d}(x,y)$ is the normalized spatial nonlinear coefficient distribution with $\max[\bar{d}(x,y)] = 1$. From Eq. (1) we note that when $\sqrt{\eta_{\text{nor}} P_p L} = \pi/2$, $\eta = 1$ and all the input signal photons at ω_1 have been converted to ω_2 . The pump power required to reach maximal conversion is $P_{\text{max}} = (\pi/2L)^2/\eta_{\text{nor}}$.

The initial demonstrations of upconversion SPDs for the 1.55 μm spectral region used bulk PPLN samples and either ns pulses [6] or resonant cavities [9] but were not able to reach the high pump powers required for maximum conversion. By using waveguide nonlinear devices, owing to tight confinement of the interacting modes over lengths of several cm, it was possible to reduce P_{max} from 35 W in [9] to 105 mW [8]. Subsequent experiments went on to demonstrate that the upconversion process preserved phase coherence [10] and entanglement properties [11] of the input signal. Recently, upconversion of single-photons at 1304 nm from semiconductor quantum dots was demonstrated as well [12]. Upconversion has also been used to erase the frequency distinguishability of two single photons [13], and has been shown to preserve photon statistics out to fourth order [14].

An issue plaguing most implementations of upconversion single-photon detectors for 1550-nm signals are noise counts generated due to spontaneous scattering processes of the strong pump. A pump photon scattered into the phasematching acceptance bandwidth of the device will be efficiently upconverted and registered as a signal. A schematic of noise processes in QFC devices is shown in Fig. 1. Of the order 10^{18} pump photons s^{-1} are required for maximum conversion, so even extraordinarily weak scattering processes induce noise count rates prohibitively high for applications in quantum communication. The two primary noise processes are spontaneous parametric downconversion (SPDC) and spontaneous Raman scattering (SRS). It has been shown that random duty-cycle errors inherent in the fabrication of quasi-phase-matching (QPM) gratings by periodic poling result in a phasematching pedestal, so that parasitic mixing processes nominally strongly phase-mismatched in an ideal QPM grating experience considerably enhanced conversion efficiency [15]. In QFC systems with short-wavelength pumps, the QPM pedestal results in a statistically white SPDC noise floor for essentially all wavelengths longer than the pump within the transparency window of the material, and has been shown

to be the dominant noise source in QFC systems with large negative signal-pump frequency separations $\Delta\omega = \omega_1 - \omega_p$ [16]. In Sec. 3 we will discuss the effect of varying $\Delta\omega$ on the noise.

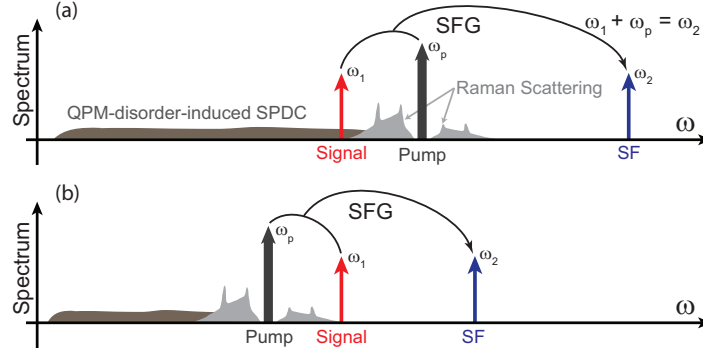


Fig. 1. Schematic of noise processes in (a) short-wavelength-pumped and (b) long-wavelength-pumped upconversion single-photon detectors.

As Fig. 1 shows, the choice of pump wavelength for an upconversion detector has a major impact on the noise performance of the device. SPDC can only produce noise photons at frequencies lower than the pump, and therefore will only affect short-wavelength-pumped upconverters. SRS can produce photons either red- or blue-shifted from the pump as Stokes or anti-Stokes sidebands, which are generated with an intensity ratio determined by a Boltzmann factor owing to the thermal occupation of phonons [17]. The ratio of the rate R_{aS} of anti-Stokes Raman photons for a medium pumped at ω_a to Stokes photons R_S for a medium pumped at ω_b , with $\omega_b - \omega_a = \Delta\omega$, is given by

$$\frac{R_{aS}}{R_S} = \left(\frac{\omega_b}{\omega_a}\right)^3 \exp\left[-\frac{\hbar\Delta\omega}{kT}\right]. \quad (4)$$

It was shown in [8] that for an upconversion detector with $\lambda_p = 1.32 \mu\text{m}$ and $\lambda_1 = 1.55 \mu\text{m}$, the ratio of noise counts is consistent with this Boltzmann factor when the roles of the signal and pump are interchanged. However, the spectral dependence of the Raman effect was not investigated. SRS was also the major noise source in a recent experiment aimed at downconversion of single photons from diamond color centers into the $1.5\text{-}\mu\text{m}$ telecom band [18], but their SRS measurements did not explore the large-frequency-shift regime, which is important for this work. In Sec. 3, we will show that Raman scattering is a major noise source even at frequency shifts well past the locations of LiNbO_3 Raman peaks.

To enable low-noise upconversion detection (or any high-fidelity QFC process), one must choose a pump wavelength that does not introduce noise via SPDC or SRS [16]. As Fig. 1(b) shows, this constraint requires pump frequencies ω_p substantially lower than the signal ω_1 . We term the “dark count” rate due to spontaneous scattering processes to be the noise-count rate (NCR) of the system to distinguish it from the intrinsic dark count rate (DCR) of the SPD, which arises from processes within the semiconductor device. There have recently been demonstrations of long-wavelength-pumped upconversion detectors for both the $1\text{-}\mu\text{m}$ and $1.55\text{-}\mu\text{m}$ spectral bands [19, 20], and long-wavelength-pumping has been shown to dramatically reduce the NCR. In what follows, we describe a tunable long-wavelength-pumped upconversion SPD. The tunable pump wavelength allows us to investigate the spectral dependence of the NCR, which was not possible in earlier work [20]. We demonstrate an upconversion efficiency of 86% using a pump wavelength which was tuned from 1796 to 1859 nm. This high upconversion efficiency enabled a total system PDE of 37%. The NCR versus $\Delta\omega$ is shown to be consistent

with measured Raman spectra of LiNbO_3 , enabling calculation of the noise-equivalent power (NEP) of the upconversion SPD versus pump wavelength. Our results are of importance not only for upconversion detectors, but for QFC devices for hybrid quantum systems and quantum networks [21], in which quantum emitters in the near-visible may be linked with telecommunications infrastructure by using a QFC interface [22].

2. Experimental setup and characterization

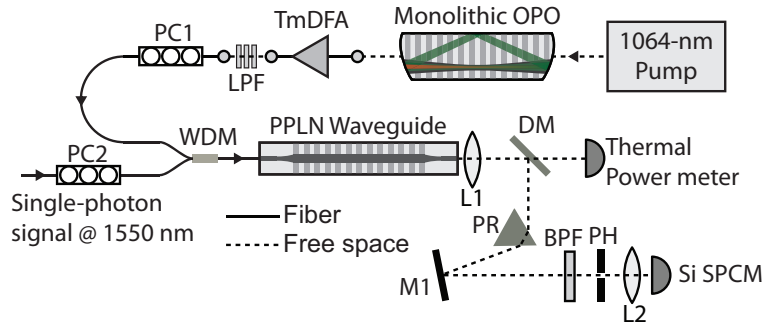


Fig. 2. Experimental setup for the long-wavelength-pumped upconversion detector. Abbreviations: LPF, long-pass filter; PC, polarization controller; WDM, wavelength division multiplexer; DM, dichroic mirror; PR, prism; BPF, band-pass filter; PH, pinhole.

The experimental setup for our long-wavelength-pumped upconversion detector is shown in Fig. 2. We fabricated reverse-proton-exchanged (RPE) periodically poled lithium niobate waveguides designed for sum-frequency generation of an 1850-nm pump and 1550-nm signal. The waveguides had total length $L = 52$ mm, and were fabricated with a poling period $\Lambda_G = 18.8 \mu\text{m}$. The waveguides had at their inputs spatial-mode filters designed to match the mode size of SMF-28 optical fiber, and were fiber-pigtailed with coupling losses of approximately 0.8 dB. We measured propagation losses below 0.2 dB cm^{-1} using the Fabry-Perot technique [23]. The waveguide facets were flat-polished and antireflection coated to eliminate interference effects and improve the sum-frequency (SF) throughput. The waveguides were held in a temperature-controlled oven.

The tunable pump source we used for this experiment was based on a monolithic PPLN optical parametric oscillator (OPO) [24]. The OPO cavity was formed from a $52 \times 5 \times 1$ mm periodically poled congruent LiNbO_3 chip with off-axis spherical polish ($R = 40$ mm) that supported a triangle-shaped closed optical path consisting of bounces off the two spherical facets at a slight angle followed by a total-internal-reflection bounce off the side of the chip. The OPO was pumped by a 1064-nm Yb-doped fiber laser and amplifier, and had an oscillation threshold of approximately 1 W. The OPO could produce up to 0.96 W of signal power tunable in a narrow (less than 4 GHz FWHM, instrument limited) signal line between 1.76 and $1.94 \mu\text{m}$ in a temperature range of 130 to 200°C [24]. For stability, we operated the OPO close to threshold, and used the narrow linewidth signal wave to seed a Tm-doped fiber amplifier (TmDFA) which could produce up to 800 mW of output power.

The 1550-nm-band signal was produced by a tunable external-cavity diode laser and a series of calibrated attenuators. As PPLN RPE waveguides support only TM-polarized modes, polarization controllers were used to rotate the polarization of both the signal and pump beams. If necessary, polarization-independent upconversion detectors as in [25] could be built in the future. The long-wavelength pump and single-photon-level signal were combined off-chip in a micro-optic C/L-band WDM (Oplink) found to have low insertion loss for both the signal and

pump wavelengths. For measurements of the detection efficiency, the signal level was set to 10^6 photons s^{-1} at the entrance of the WDM. The upconverted SF at ω_2 was collected by an aspheric lens ($f = 8$ mm). The pump and signal were separated from the SF by a dichroic mirror and the pump power was monitored using a thermal power meter. The upconverted output was further filtered using a brewster-angle prism and 50-nm-bandwidth optical bandpass filter to reject parasitic second harmonic radiation of the strong pump. The SF was focused onto a Si single-photon-counting module (Perkin-Elmer SPCM-AQR-13) [26]. The transmission of the optical system between the waveguide output facet and the SPCM was 92%.

2.1. Waveguide characterization

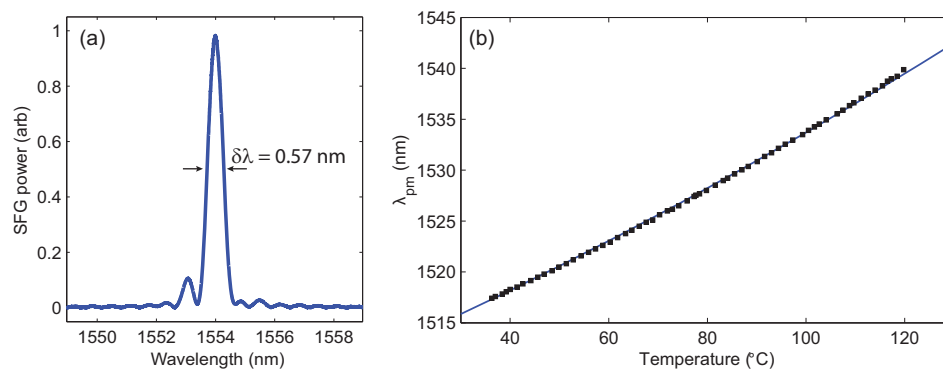


Fig. 3. (a) Phasematching tuning curve for a 52-mm-long PPLN waveguide, $\lambda_p = 1800$ nm; (b) Temperature tuning data (squares) and fit to LiNbO₃ dispersion [27], showing 0.27 nm/°C tuning rate.

We first characterized the phasematching of the upconversion waveguides. A phasematching tuning curve is shown in Fig. 3(a). The pump wavelength λ_p was fixed at 1800 nm and the signal wavelength was swept. We observed a phasematching FWHM of 0.57 nm, which matches the expected width calculated from the LiNbO₃ dispersion relations [27] and the 47-mm QPM grating length. We also measured the temperature tuning of the phasematching, which is shown in Fig. 3(b). Experimental data are represented as squares and the solid curve is a theoretical calculation based on a temperature-dependent Sellmeier relation for LiNbO₃ [27]. The phasematching temperature tuning rate for $\lambda_p = 1800$ nm was 0.27 nm/°C.

We measured the conversion efficiency of the waveguide as a function of both pump power P_p and signal wavelength λ_1 for a constant classical-level input signal power of 20 μ W; the results are shown in Fig. 4(a). We reach a maximum internal conversion efficiency η of 86% which is consistent with our observed propagation losses of 0.17 dB cm^{-1} at λ_1 and a value of 0.1 dB cm^{-1} at λ_2 and our observed 41 dB (99.99%) signal depletion. Measurements at 24 pump powers between 0 and 350 mW have been interpolated to provide a smooth plot. Figure 4(b) shows a theoretical prediction of the internal conversion efficiency calculated by numerically integrating the coupled-wave equations for SFG with our experimental parameters [28]. There is good agreement of the major features and the observed theoretical and experimental conversion efficiencies match very well. Figure 4(c) shows a slice of the two-dimensional data at the QPM peak. The data (squares) are well fit by Eq. (1), with $\eta_{\text{hor}} = 68\% \text{ W}^{-1} \text{ cm}^{-2}$ and thus $P_{\text{max}} = 151$ mW.

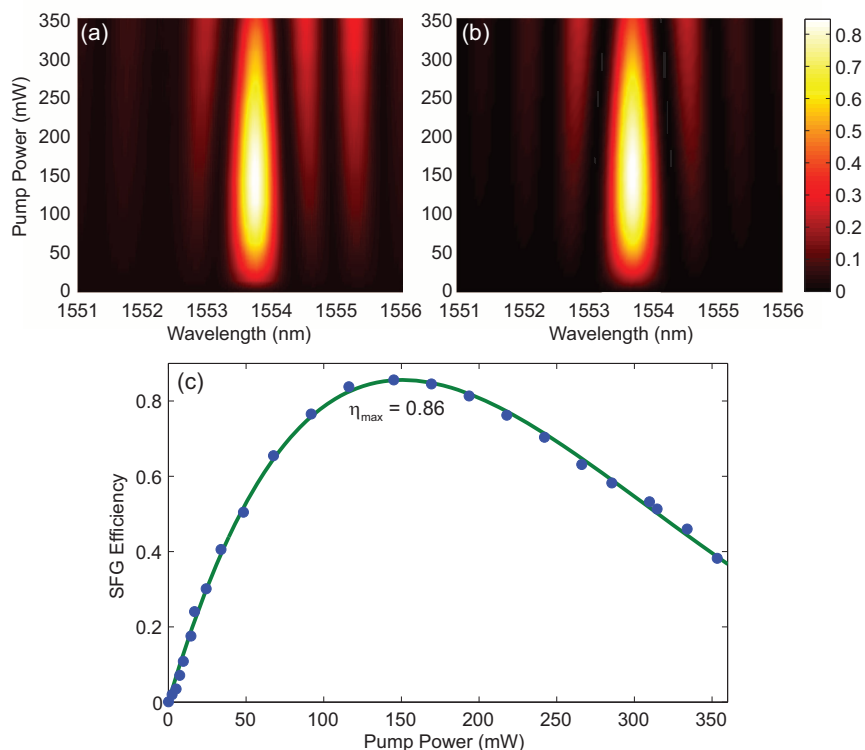


Fig. 4. (a) Experimentally observed and (b) numerically predicted conversion efficiency versus pump power and signal wavelength. Simulation parameters: α_1 (α_2) = 0.17 (0.1) dB cm⁻¹, and P_{\max} = 151 mW; (c) internal conversion efficiency of PPLN waveguide (λ_1 = 1554 nm, λ_2 = 834 nm).

2.2. Single-photon performance

We next characterized the performance of the detection system by attenuating the signal laser to a level of 10^6 photons s⁻¹ at the input of the WDM using a series of calibrated fiber-optic attenuators. Before inserting the long-pass filters into the pump path, a strong noise signal overwhelmed the upconversion of the signal light, saturating the SPCM. We investigated the noise spectrum of the TmDFA by separating the long- and short-wavelength components using a C/L-band micro-optic WDM and coupling the C-band components into an optical spectrum analyzer. The TmDFA noise spectrum is shown in Fig. 5 for a 3-mW seed at 1800 nm and output power of 700 mW. The TmDFA is pumped by an Er: fiber laser at 1567 nm [29], but a shelf of spontaneous emission noise is observed at all wavelengths down to approximately 1470 nm. Another popular pump scheme for Tm lasers is to pump at 790 nm; a subsequent cross-relaxation process enables the generation of two laser photons for each pump photon. Investigation of cross-relaxation Tm lasers also shows C-band spontaneous emission [30]. For low-noise upconversion, the pump light and spontaneous emission must be filtered. Previous work on upconversion using Tm laser systems used fiber-optic WDMs as filters [20]. Here, we use a series of 3 free-space long-pass filters placed into a fiber bench to achieve the very high extinction (> 100 dB) needed to eliminate noise due to SFG of noise photons due to pump processes with the strong long-wavelength pump. With our devices tuned to a phasematched

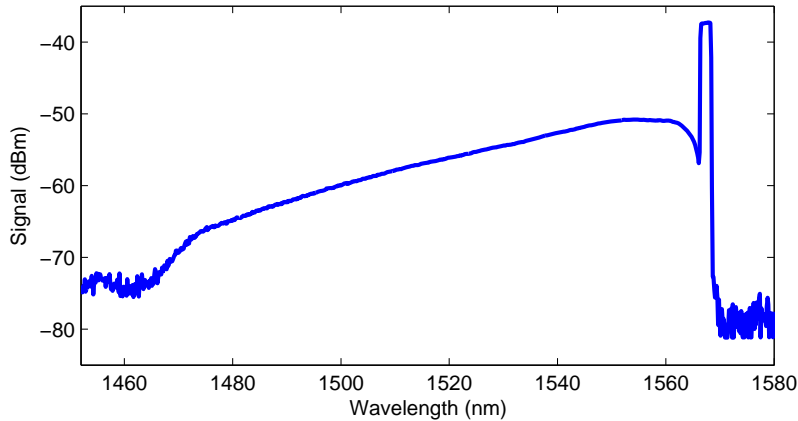


Fig. 5. TmDFA noise spectrum between 1450 and 1580 nm, measured by an optical spectrum analyzer with a resolution bandwidth of 2 nm, showing the TmDFA pump line at 1567 nm and shelf of spontaneous emission down to approximately 1470 nm.

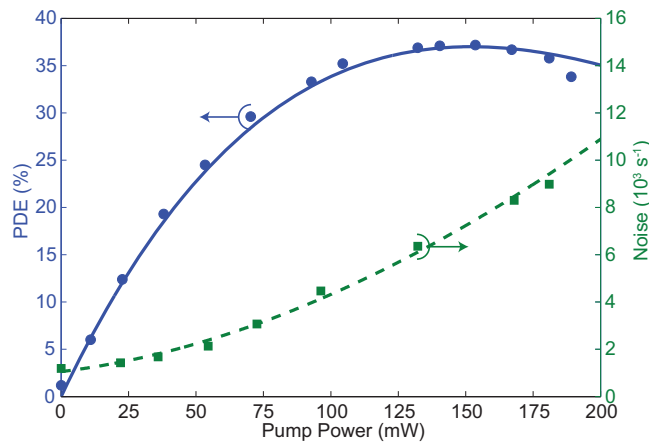


Fig. 6. Left axes: measured photon detection efficiency with $\lambda_p = 1810$ nm (circles) and fit to Eq. (1); right axes: measured noise count rate (squares) and polynomial fit (dashed).

wavelength of 1555 nm, the phasematching acceptance bandwidth of the upconverter is itself a very effective filter of the 1567-nm TmDFA pump; we observe 50 dB rejection of upconversion of the 1567-nm noise photons versus 1555 nm signal photons, which is consistent with a prediction based on a domain-disorder-induced QPM pedestal [15].

After blocking the pump noise with long-pass filters, we could measure the photon detection efficiency (PDE) and noise count rate (NCR) of our upconversion detector. Measurements were made using several pump wavelengths between 1796 and 1859 nm. A plot of the PDE (left axes) and NCR (right axes) versus pump power for a pump wavelength $\lambda_p = 1810$ nm is shown in Fig. 6. At $P_p = P_{\max}$ we attain a maximum PDE of 37%. The measured conversion efficiency matches our expected conversion efficiency by combining the losses of each component, as shown in Table 1. While the SPCM datasheet quotes an expected PDE of 55% at 834 nm, we find that a value of 57% is needed to explain our observed system detection efficiency. With technologically feasible improvements to the setup and waveguide, and a detector with PDE $\eta_Q = 57\%$, we should be able to obtain an internal conversion efficiency of 94% and a

Table 1. Loss and transmission of upconversion detector components. The column with feasible transmission values is based on idealized optical components and improved waveguides with pigtailling losses of 0.5 dB and propagation losses of 0.1 dB cm⁻¹.

Component	Loss (dB)	Transmission	Feasible T
Wavelength combiner	0.45	0.97	0.99
Fiber pigtailling	0.8	0.83	0.9
Conversion efficiency	0.66	0.86	0.94
Optical system	0.36	0.92	0.99
SPCM PDE	2.4	0.57	η_Q
		Total:	$0.83\eta_Q$

maximum PDE of 45%.

3. Spontaneous Raman scattering and noise

As seen in Fig. 6, there are still appreciable noise counts for $\lambda_p = 1810$ nm. This result contrasts with earlier work involving and 1810-nm-pumped upconversion detector [20]. In [20], there was insufficient pump power (only 60 mW was coupled into the waveguide) to reach P_{\max} , and, perhaps more importantly, the SFG output was passed through a monochromator before being routed to the SPCM, significantly narrowing the spectrum of detected photons. We estimate the bandwidth of our output filtering system to be approximately 20 nm. This was narrow enough to reject any pump second-harmonic generation, but not narrow enough to filter the upconverted signal (with linewidth of a few MHz) from any upconverted SRS photons (which will fill the 74-GHz (0.57-nm) upconversion acceptance bandwidth).

In order to quantify the expected spectral dependence of the noise resulting from spontaneous Raman processes, we measured the Raman spectrum of a congruent LiNbO₃ sample using a Raman microscope (WiTec Alpha300 S). We used a 514-nm Argon-ion laser as an excitation source and performed measurements in the $x(zz)\bar{x}$ geometry; the results are shown in Fig. 7(a). Measurements were taken with an 1800-lines/mm grating at two different positions to reconstruct the large spectral range. The background counts of the Peltier-cooled detector have been subtracted. Naively, one expects the Raman spectrum for a complex material with several Raman-active phonons to be a sum of the Lorentzian responses for each of the modes [31]. Along with the measured data we plot a fit to such a sum-of-Lorentzians (green curve), from which we see that a significant deviation from Lorentzian behavior occurs at large frequency shifts. To the best of our knowledge, this large-shift SRS “shelf” has not been analyzed elsewhere in the literature on LiNbO₃. We initially suspected the shelf might be due to the high defect density in congruent LiNbO₃ (which is 1.7% Li deficient) when compared with a stoichiometric crystal. Since stoichiometric LiNbO₃ is not readily available, we tested this hypothesis by comparing congruent-composition LiTaO₃ against stoichiometric LiTaO₃. The stoichiometric LiTaO₃ showed a similar shelf as congruent LiTaO₃, suggesting that disorder is not important to the existence of the shelf. We also measured planar RPE waveguides processed under similar conditions to the waveguides used in the upconversion detector with sufficient spatial resolution to identify differences in the Raman behavior of the protonated versus non-protonated regions in the sample, and did not see any quantitative differences in the Raman behavior. Further work will be required to uncover the origin of the shelf.

We next sought to compare the observed noise counts with a prediction based on the measured Raman spectrum. The Raman spectrum in Fig. 7(a) was measured in the Stokes configuration. We can use the measured spectrum in combination with the relationship between

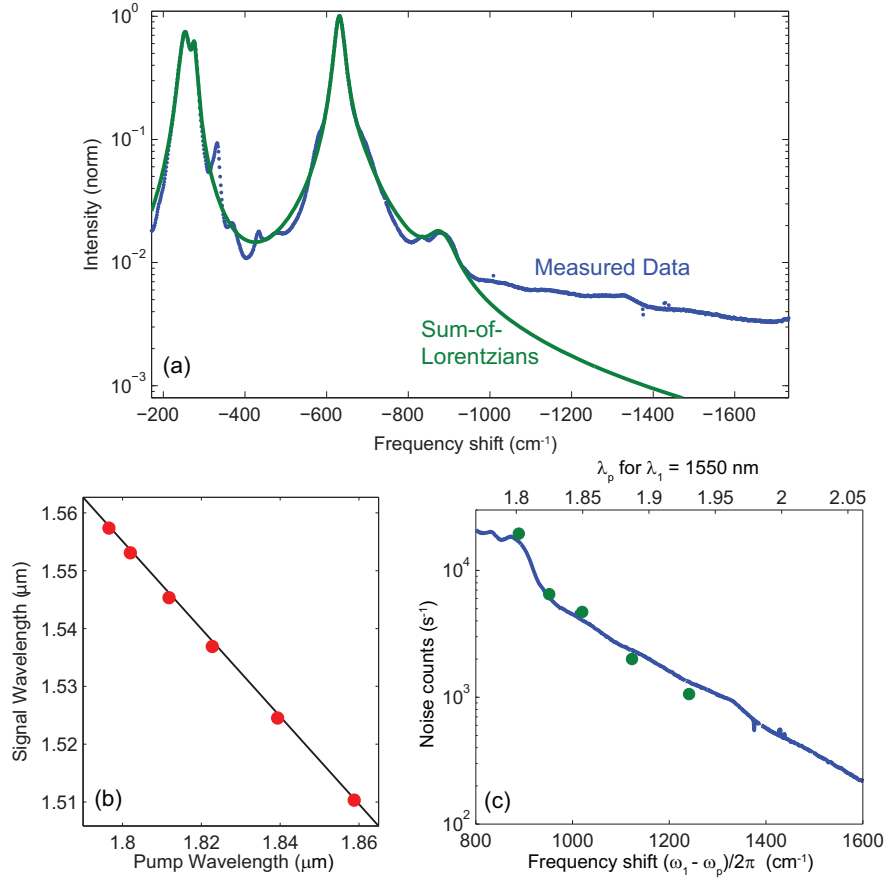


Fig. 7. (a) Measured Raman spectrum of LiNbO₃ (blue dots) and fit to a sum of Lorentzians (green solid); (b) Tuning of upconversion waveguide: phasematched signal wavelength λ_1 versus pump wavelength λ_p ; (c) Measured NCR at peak PDE versus signal-pump frequency difference $\Delta\omega$ and, equivalently, pump wavelength needed for upconversion of $\lambda_1 = 1550$ nm, with theoretical fit to anti-Stokes SRS noise photon generation.

Stokes and anti-Stokes scattering to compute the expected noise photon rate due to anti-Stokes SRS [32]. The scattering rate into a bandwidth $\delta\omega$ around ω_1 in a waveguide of length L can be shown to be

$$N_1 = \frac{8\pi^2}{3} \frac{c^2 n_p}{\omega_1^3 \hbar \omega_p n_1^2} \left(\rho e^{-\hbar\Delta\omega/kT} g_L(\Delta\omega) \frac{d\sigma}{d\Omega} \Big|_0 \right) \theta_R P_p L \delta\omega, \quad (5)$$

where ρ is the number density of unit cells, $g_L(\Delta\omega)$ is the Raman lineshape function, $d\sigma/d\Omega|_0$ is the scattering cross section, and the overlap integral for the Raman interaction is

$$\theta_R = \iint |u_1(x,y)|^2 |u_p(x,y)|^2 dx dy. \quad (6)$$

As mentioned in Sec. 2.2, we measured the PDE and noise counts for a series of pump wavelengths between 1796 and 1859 nm. The waveguide was held at a constant temperature of 30 °C, and the phasematched signal wavelength followed the trajectory shown in Fig. 7(b). The

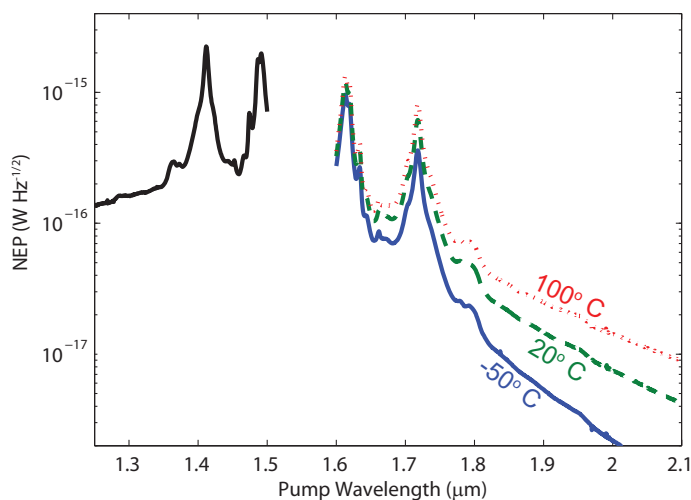


Fig. 8. Noise equivalent power (NEP) of a 1.55 μm upconversion detector pumped between 1.2 and 2.1 μm , based on Perkin-Elmer SPCM and operated at temperatures between -50 and 100°C .

noise counts at peak PDE are plotted in Fig. 7(c); the SPCM intrinsic DCR of 480 counts s^{-1} was subtracted to isolate the noise contribution due to the frequency conversion process. The solid curve is a calculation of the anti-Stokes Raman noise based on Eq. (5) where $P_p = P_{\text{max}}$. We take the scattering cross section $d\sigma/d\Omega|_0$ to be an adjustable parameter, and see that the spectral variation of the noise counts is consistent with a prediction based on our measured Raman spectrum which incorporates the non-Lorentzian shelf at large frequency shifts.

A common figure of merit for single-photon detectors is the noise-equivalent power (NEP), defined as the optical power for which a 1-second integration gives a unity signal-to-noise ratio:

$$\text{NEP} = \frac{hc}{\lambda \text{PDE}} \sqrt{2\text{NCR}}. \quad (7)$$

For an upconversion SPD for 1.55- μm photons dominated by Raman-induced noise counts we can calculate the NEP as a function of pump wavelength, based on the results shown in Fig. 7(c). This was done by using values of PDE from the SPCM datasheet [26] and the Raman spectrum fit in Fig. 7(c), which provides the Raman-attributed NCR versus λ_1 . We plot the results in Fig. 8 for both short- and long-wavelength-pumped upconverters operated at temperatures between -50°C and 100°C . One should note that for pump wavelengths shorter than 1.3 μm , a significant source of noise counts will be QPM-disorder-enhanced non-phasematched parametric fluorescence [16], which is not included here. The noise can be reduced substantially by operating the upconverter below room temperature. For example: by cooling to -50°C (within the range of Peltier coolers) in combination with a 1.9- μm pump, the noise could be reduced by a factor of approximately 7.4. Using our measured Raman data, the NEP is easily calculable for any single-photon detector of interest.

We note that in our experiment no special effort was made to spectrally filter the upconverted signal beyond rejection of parasitic pump SHG. In an earlier experiment demonstrating low-noise upconversion detection pumped at 1810 nm, noise performance near the DCR of the SPD was achieved by filtering the upconverted light using a monochromator, at significant expense on the system throughput. In most applications, the signal of interest will have substantially smaller bandwidth than the acceptance bandwidth of the upconverter (74 GHz (0.57 nm) for

5-cm-long RPE PPLN waveguide at 1.55 μm). Because upconverted SRS noise will fill the acceptance bandwidth while the signal will presumably be narrowband, the noise can be significantly reduced by spectral filtering. High-diffraction-efficiency holographic gratings with minimal losses have been used as post-upconversion filters in a recent publication [33].

4. Conclusion

We have demonstrated upconversion single-photon detection for the 1.5- μm telecom band pumped by an OPO. We achieved an input signal depletion of 41 dB, which yielded an internal conversion efficiency $\eta = 86\%$ limited by propagation losses of the waveguide. The total system photon detection efficiency was 37%, with 45% possible with technological improvements. We analyzed the noise behavior of the upconversion detector and found it to be consistent with measurements of the LiNbO_3 Raman spectrum.

Upconversion detection is a promising technique to extend the use of well-developed silicon single-photon detectors for photon-counting applications in the telecommunications band. However, noise sources due to domain-disorder-enhanced parametric processes and spontaneous Raman scattering must be understood and managed. By using pump wavelengths substantially longer than the input signal, using narrowband optical filtering of the sum-frequency output, and cooling the LiNbO_3 waveguide, it is possible to obtain noise performance very close to the intrinsic dark-count rate of Si detectors. These results will also be important more broadly in frequency conversion systems for quantum networks, in which the elimination of noise processes will be important for the faithful frequency translation of quantum states.

Acknowledgments

J. S. P. was supported by a Robert N. Noyce Stanford Graduate Fellowship. Additional support was provided by the United States AFOSR under grant FA9550-09-1-0233 and by the National Institutes of Standards and Technology (NIST) quantum information initiative. We also acknowledge the support of Crystal Technology, Inc. The identification of any commercial product or trade name does not imply endorsement of recommendation by NIST.